Received: 23 June 2021 | Revised: 24 August 2021 | Accepted: 25 August 2021

DOI: 10.1111/jace.18118

Journal of American Ceramic Society

RESEARCH ARTICLE

Room-temperature dislocation plasticity in $SrTiO_3$ tuned by defect chemistry

Stephan Stich[1] | Kuan Ding[1] | Qaisar Khushi Muhammad[1] | Lukas Porz[1] | Christian Minnert[1] | Wolfgang Rheinheimer[1,2] | Karsten Durst[1] | Jürgen Rödel[1] | Till Frömling[1] | Xufei Fang[1]

[1] Department of Materials and Earth Sciences, Technical University of Darmstadt, Alarich-Weiss-Str. 2, Darmstadt 64287, Germany

[2] Forschungszentrum Jülich GmbH, Wilhelm-Johnen-Straße, Jülich 52428, Germany

Correspondence
Xufei Fang, Department of Materials and Earth Sciences, Technical University of Darmstadt, 64287 Darmstadt, Germany.
Email: fang@ceramics.tu-darmstadt.de

Funding information
Athene Young Investigator Programme at TU Darmstadt; Deutscher Akademischer Austauschdienst, Grant/Award Number: 91669061

Abstract

Dislocations have been identified to modify both the functional and mechanical properties of some ceramic materials. Succinct control of dislocation-based plasticity in ceramics will also demand knowledge about dislocation interaction with point defects. Here, we propose an experimental approach to modulate the dislocation-based plasticity in single-crystal $SrTiO_3$ based on the concept of defect chemistry engineering, for example, by increasing the oxygen vacancy concentration via reduction treatment. With nanoindentation and bulk compression tests, we find that the dislocation-governed plasticity is significantly modified at the nano-/microscale, compared to the bulk scale. The increase in oxygen vacancy concentration after reduction treatment was assessed by impedance spectroscopy and is found to favor dislocation nucleation but impede dislocation motion as rationalized by the nanoindentation pop-in and nanoindentation creep tests.

KEYWORDS

defect chemistry engineering, dislocation plasticity, nanoindentation, oxygen vacancy, strontium titanate

1 | INTRODUCTION

Dislocations in ceramics have the potential to impact both functional and mechanical properties. On the one hand, dislocations in various oxides have demonstrated potential to tune electrical conductivity, thermal conductivity,[3–5] dielectric and piezoelectric properties.[6] On the other hand, dislocations can be introduced into ceramics to improve plasticity[7–10] and fracture toughness.[11–13] These new endeavors modify the conventional belief that ceramics are brittle, exhibiting little or no dislocation-mediated plasticity at room temperature. The strong ionic/covalent bonds and the large Burgers vectors in most ceramics are deemed to render them having high strength but little plasticity and low fracture toughness.

To improve dislocation-based plasticity and to pave the road for tuning dislocation-based functional and mechanical properties, dislocation behavior (dislocation nucleation, multiplication, and motion) needs to be better understood in ceramics. Similar to metallic materials, it has been recognized that the low density of dislocation sources (e.g., low pre-existing dislocation density) in ceramics can be a critical factor that hinders large plasticity[14,15] or triggers the brittle-ductile transition.[16] Therefore, a reasonable approach to improve dislocation plasticity in ceramics is by increasing the pre-existing

dislocation density. For example, Stokes et al.[17] demonstrated that the tensile strength of single-crystal MgO with sprinkled surfaces used to generate a high density of new dislocations was decreased by a factor of ~14, compared to a well-polished sample annealed at 2000°C.

Recently, Nakamura et al.[9] demonstrated that the room-temperature bulk plasticity of single-crystal $SrTiO_3$ can be manipulated by changing the Sr/Ti ratios (1.00 and 1.04) in the starting powders. It was assumed that changing the composition yields samples with different Sr vacancy concentrations, which may have resulted in the different plastic behavior.[9] Our further examination of these samples shows different pre-existing dislocation densities and oxygen vacancy concentrations in such samples as well.[10] Compared to samples with Sr/Ti = 1.00 (with a pre-existing dislocation density ~10^{10} m^{-2}), the samples with Sr/Ti = 1.04 in the starting powders have a higher pre-existing dislocation density (~10^{11} m^{-2}) and exhibit lower yield strength (~15% decrease) and much higher fracture strain (~70% increase).[9] Using the same materials and chemical treatment, the current authors revealed the underlying mechanisms via nanoindentation studies.[10] Contrary to the dislocation nucleation-dominated incipient plasticity at the nanoscale, dislocation motion and multiplication[12,15] plays a more important role in plasticity at micro- and larger scale.[18]

In addition to the different pre-existing dislocation densities in those samples, the point defect concentrations were found to differ with the Sr/Ti = 1.00 sample giving a higher oxygen vacancy concentration. As various types of defects could act as dislocation sources and promote heterogeneous dislocation nucleation,[14] it is thus of great interest to discern the effect of pre-existing dislocations from that of point defects. Point defects such as vacancies and interstitials play critical roles in the functional properties in ceramics (e.g., in defect chemistry studies),[19,20] yet their effect on the mechanical properties of ceramics, particularly dislocation-based mechanics, is much less investigated. Regardless of the theoretical prediction,[21] little effort has been made using point defects to tune the incipient plasticity in ceramics[22] as compared to metallic materials.[23,24] A pertinent question would be: How is plasticity affected by point defects such as oxygen vacancies in ceramics?

On the one hand, it has been proposed that point defects are favorable for dislocation nucleation.[25,26] In order to capture dislocation nucleation, nanoindentation pop-in tests are most feasible.[27–29] Here, the term "pop-in" refers to the displacement jump at a normally constant load in a load-controlled indentation system, indicating the transition from elastic to plastic deformation. The pop-in phenomenon has been widely observed in metallic materials with low pre-existing dislocation density.[18,28,30] For various oxides with low surface dislocation density, we validated that purely dislocation-dominated pop-in events occur when the indenter tip radius is smaller than a certain value depending on the materials and testing conditions.[31]

On the other hand, point defects could act as local barriers to impede dislocation motion.[32,33] In order to assess the dislocation motion, nanoindentation creep tests[34–36] can be adopted. Furthermore, in order to establish an experimental protocol bridging the macroscale (bulk compression)[9] and nano-/microscale (nanoindentation)[10] testing, we have previously discussed the similarities and differences between bulk compression and nanoindentation tests.[37] To this end, bulk compression tests are also carried out in this work to compare with the nanoindentation tests.

To address the impact of point defects on dislocation plasticity in ceramics, in this work, we focus on the effect of oxygen vacancies on dislocation-mediated plasticity in single-crystal $SrTiO_3$. We first perform reduction treatments on single-crystal $SrTiO_3$ to increase the oxygen vacancy concentration as evidenced by impedance spectroscopy. Nanoindentation and bulk compression tests are then performed on the reduced and reference samples (without reduction treatment). The incipient plasticity in nanoindentation tests and the yield strength of the bulk samples are compared and analyzed. In addition, nanoindentation creep tests are performed to reveal dislocation mobility at room temperature.

2 | EXPERIMENTAL PROCEDURE

2.1 | Sample preparation

Single-crystal $SrTiO_3$ (0.05% wt. Fe-doped, Alineason Materials Technology) was used as sample material for compression and nanoindentation testing. The samples were pre-polished from the manufacturer, followed by a fine vibrational polishing performed with a water-based solution containing 0.04-μm colloidal silica (OP-S, Struers) to remove the surface mechanical deformation layer prior to the nanoindentation tests. For nanoindentation tests, the sample surface was examined before and after the reducing treatment using atomic force microscopy (AFM, Veeco Plainview). Average surface roughness of less than 2 nm was assured, and no clear change of surface topography was observed. For bulk compression tests, the samples were cut from a single crystal (4 × 4 × 8 mm) into smaller samples (~2 × 2 × 4 mm) using a wire saw, and the surface of the smaller samples were gently polished to remove the major surface damage during cutting.

Compared to the reference $SrTiO_3$ sample, the oxygen vacancy concentration of the reduced samples is increased

by a reduction treatment in forming gas (Ar + 2.4% H_2) and in pure N_2 at 700°C (heating and cooling rate 5°C/min) for 24 h in order to generate oxygen vacancies.[38] Furthermore, a qualitative verification of the reduction state is afforded by impedance spectroscopy. In the following sections, samples will be labeled as STO-Ref, STO-H_2, and STO-N_2, corresponding to the three conditions for sample treatment.

2.2 | Impedance spectroscopy

To elucidate the state of reduction in the reference and reduced samples, impedance measurements were conducted (with a sample dimension of about 4 × 4 × 1 mm) to obtain temperature-dependent electrical resistance. Platinum paste (Ferro GmbH) was applied on both sides of each sample to serve as electrode material and fired in a tube furnace at 930°C for 10 min. To achieve uniform electrodes and to avoid bubble formation in the platinum paste, controlled heating and cooling rates were used. Temperature-dependent impedance spectroscopy was conducted in a tube furnace equipped with an impedance analyzer (Novocontrol), in the frequency range of 0.1 Hz to 1 MHz, with an amplitude of 0.1 V in the temperature range of 100 to 700°C. The impedance data were evaluated with the RelaxIS software (rhd instruments).

2.3 | Nanoindentation tests

Nanoindentation tests were performed on the same thin samples in Section 2.2 prior to the impedance measurements on the (001) surface, that is, on the 4 x 4 mm surface. The choice of (001) surface is made as it can be chemically etched to reveal the dislocations. Nanoindentation pop-in and creep tests were conducted with a diamond Berkovich tip (Synton-MDP) with the iNano system (Nanomechanics Inc.). At least 25 indents were performed for the pop-in study for each condition with a constant indentation strain rate of 0.02 s^{-1}. The spacing between the indents was set as 10 and 50 μm for the Berkovich tip and large spherical tip, respectively. In both cases, the spacing was about 80–100 times the maximum depth to avoid possible overlap of the plastic zones.

To obtain the indentation creep data, the constant load hold method was adopted,[35,39] with 10 repetitive tests performed for each experimental condition. After a loading segment with a constant strain rate of 0.02 s^{-1} to a peak load of 3 mN, the applied load was then held constant for 500 s before unloading. The peak load of 3 mN was selected to ensure that no cracks were induced in the samples.[40] The tip area function and frame stiffness were calibrated on fused silica according to the Oliver–Pharr method.[41]

2.4 | Bulk compression tests

Bulk compression tests were performed on single-crystal $SrTiO_3$ specimens (~ 2 x 2 x 4 mm) along the [001] direction down the long axis at room temperature, in a load frame (Z010 Zwick/Roell) using a constant strain rate of 10^{-4} s^{-1}.

2.5 | Surface characterization

After the mechanical tests, the (001) surfaces were chemically etched in 15 ml. 50% HNO_3 with 16 drops of 50% HF for ~20 s to reveal the dislocation patterns on the surface. The surface and etch pit patterns were characterized in a scanning electron microscope (SEM, Tescan Mira3-XMH) with an acceleration voltage of 5 kV. A thin carbon layer was deposited onto the sample surface to reduce the charging effect during SEM imaging. The surface characterization of the reference and reduced samples gives an identical pre-existing dislocation density of ~10^{10} m^{-2} for all samples.

3 | RESULTS AND ANALYSES

3.1 | Impedance spectroscopy measurements

The oxygen vacancy concentration in the reduced $SrTiO_3$ samples is increased as compared to the reference samples. During the reduction step, oxygen vacancies and electrons are induced $O_O^x \rightarrow V_O^{\cdot\cdot} + 2e' + 1/2O_2$. Despite electronic conductivity being possibly dominant, oxygen vacancies are induced as well. Depending on the temperature and defect chemistry of the pristine sample, either electronic or ionic conductivity is dominant.[42] The reduction in forming gas (Ar + 2.4% H_2) is expected to be stronger than the reduction treatment in N_2. Therefore, we probed the difference in the vacancy concentrations for these two samples (STO-Ref and STO-H_2) as two extreme cases. The results in Figure 1A verify that the reference sample has higher electrical resistance (lower conductivity) at the investigated temperature. As the conductivity does not change at given temperature and oxygen partial pressures, the lower conductivity in the reference sample indicates a lower oxygen vacancy concentration. The activation energy (Figure 1B) for the reference sample determined from the Arrhenius plot (0.75 eV) points toward a contribution from ionic conduction at temperatures below 400°C.[42] The STO-H_2 sample exhibits lower activation energy (0.70 eV) and overall higher conductivity (lower resistance, Figure 1A), suggesting a change in conduction mechanism and a higher oxygen vacancy concentration. Note the error bar (standard

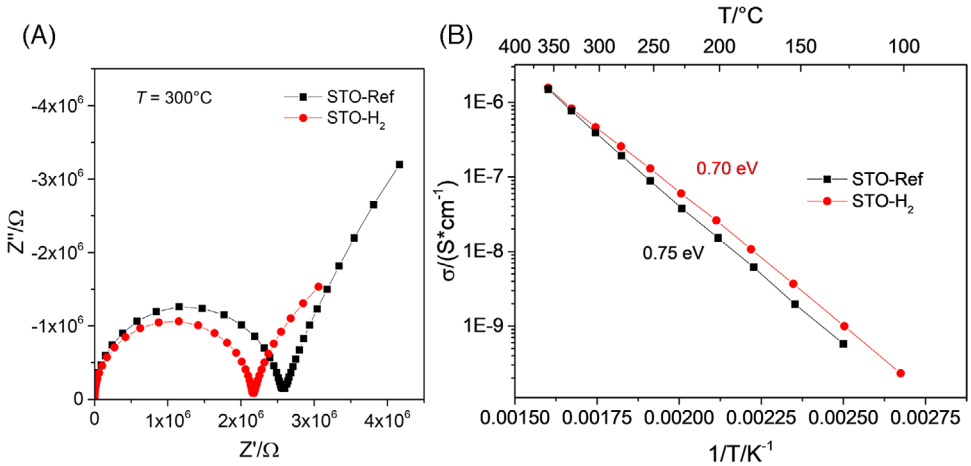

FIGURE 1 (A) Nyquist plot of impedance for the studied samples at 300°C, featuring lower resistance (higher conductivity) for STO-H_2 (B) Arrhenius plots of electrical conductivity for STO-Ref and STO-H_2 in the temperature range of 100 to 350°C

deviation) for both activation energies is about 0.004 eV, excluding the possible overlap of the activation energies for both samples. In addition, because of the rather extensive reducing atmosphere, it is likely that the material transitioned from the p- to the n-minority charge carrier regime. The increase in conductivity hints toward it because a reduction in conductivity would be expected in the case of the p-regime.[42] Moreover, it can be seen that both Arrhenius plots in Figure 1B start to overlap at higher temperatures (~350°C). This likely indicates an equilibration of the defect chemistry with the environment and the onset of chemical diffusion during the impedance measurement. It is worth noting that with impedance spectroscopy, only qualitative information can be obtained regarding the increase in oxygen vacancy concentration. To determine the exact values of the induced oxygen vacancy concentrations, one may advance to positron annihilation spectroscopy investigations, which is beyond the scope of this study.[20,43]

3.2 | Nanoindentation pop-in tests: incipient plasticity

In order to elucidate the effect of oxygen vacancy on dislocation nucleation, we first performed nanoindentation pop-in tests using a Berkovich indenter (with an effective tip radius of R = 80 nm). The representative load-displacement curves in Figure 2 illustrate the pop-in events for the same nanoindentation testing condition on STO-Ref, STO-N_2, and STO-H_2.

According to Hertzian elastic theory in contact mechanics,[28,44] the elastic deformation prior to the pop-in can be described by $P = \frac{4}{3}E_r\sqrt{R}h^{3/2}$,[28,44] where

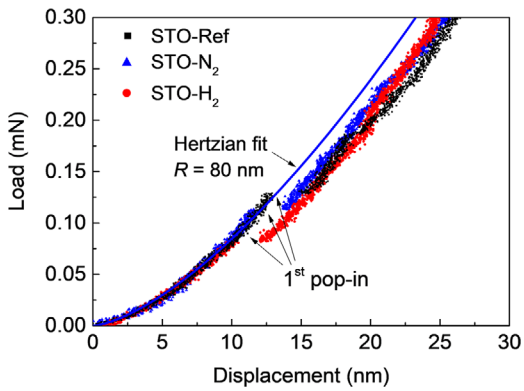

FIGURE 2 Representative load-displacement curves on STO-Ref, STO-N_2, and STO-H_2 with an effective indenter tip radius of R = 80 nm. The pop-in events are indicated by arrows and the Hertzian elastic fit by the solid blue line

P is the load, E_r the reduced modulus, h the indentation depth, and R the effective tip radius. The reduced modulus,E_r= 225 GPa, is calculated from the elastic constants of indenter and specimen by $\frac{1}{E_r} = \frac{1-\upsilon_i^2}{E_i} + \frac{1-\upsilon_s^2}{E_s}$, with E_i= 1140 GPa and υ_i= 0.07 for the diamond tip, E_s= 264 GPa and υ_s= 0.237 for $SrTiO_3$[45] assuming elastic isotropy. Note that the elastic regime before the pop-in event overlaps for the studied samples, indicating an identical elastic behavior. Furthermore, using the onset load of the first pop-in allows for the computation of the maximum shear stress,$\tau_{\max} = 0.31(\frac{6E_r^2}{\pi^3R^2}P_{pop-in})^{1/3}$.[28,44] The maximum shear stress is responsible for dislocation nucleation beneath the sharp indenter. The statistical distribution of the maximum shear stresses obtained from multiple indents for all three sample conditions is presented in Figure 3.

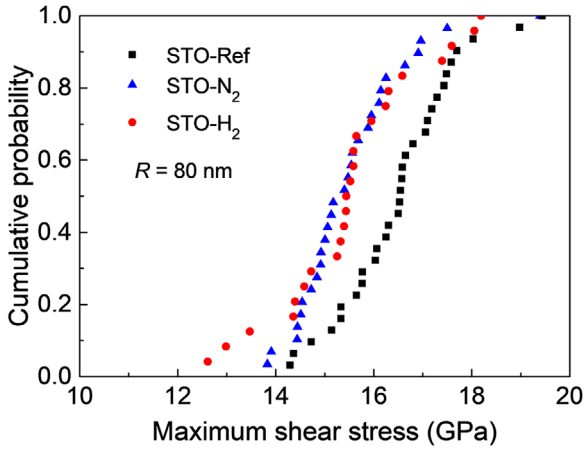

FIGURE 3 Maximum shear stress calculated at the first pop-in event for all samples treated under different conditions (i.e., STO-Ref, STO-N_2 and STO-H_2) using the same effective indenter tip radius $R = 80$ nm

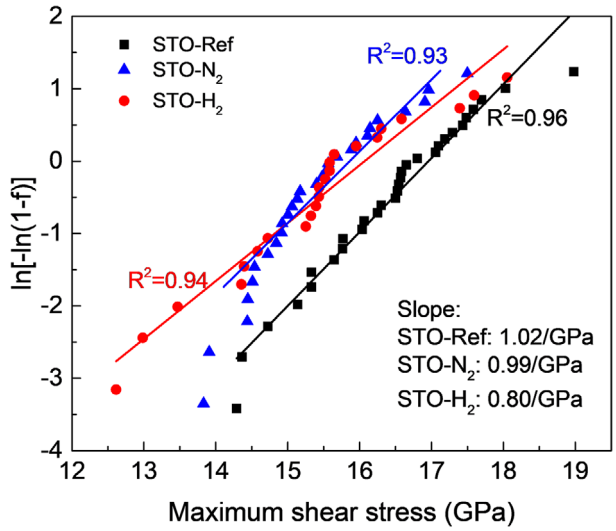

FIGURE 4 Plot of ln[-ln(1-f)] as a function of the maximum shear stress, τ, for all tested samples. The slope is determined by the linear least-squares fitting procedure. Note that for a realistic fitting, the three data points approaching the lower regime of the maximum shear stress distribution for the STO-N_2 sample have been excluded during fitting

The pop-in stress distribution in Figure 3 clearly features a decreased maximum shear stress for the reduced samples (blue triangles and red dots), compared to the reference sample (black square dots). The average maximum shear stress for the reference sample was ~16.8 GPa, which is about the theoretical shear stress estimated by $\tau_{th} \approx G/2\pi = 17\text{GPa}$, where $G = E/2(1+\upsilon)$ is used for isotropic elasticity. The close resemblance for the theoretical shear stress with the experimentally obtained maximum shear stress in the reference sample suggests homogeneous dislocation nucleation.[28,46] It is worth mentioning that Javaid et al.[47] have recently performed molecular dynamics simulations on the dislocation nucleation in single-crystal $SrTiO_3$ on the (001) surface with an indenter tip radius of 32 nm. They have reported a similar level of maximum shear stress (slightly higher than in Figure 3 due to the smaller tip radius in simulation) and observed the dislocation nucleation on the {110} plane, which is 45° inclined to the surface being indented.

For both reduced samples (STO-N_2 and STO-H_2), lower pop-in stresses with an average value of ~15 GPa were featured in Figure 3. As no change in dislocation density during the reduction process was induced, the stress distribution in Figure 3 confirms the assumption that higher content of oxygen vacancies induced by the reduction treatment facilitates dislocation nucleation and is consistent with the concept of point defects acting as possible dislocation sources.[26,33,48] It is further noted that no significant difference in pop-in stress distribution for STO-N_2 and STO-H_2 samples was observed using the indenter tip radius of $R = 80$ nm.

Considering the fact that the reduced samples were thermally treated at 700°C for 24 h during reduction treatment and then cooled down to room temperature prior to the nanoindentation tests, it is necessary to rule out the possibility that the pop-in behavior for the reduced samples was affected by the potential surface change caused by the thermal treatment. To this end, further tests on a separate sample (annealed at 700°C for 24 h in air and then cooled down to room temperature, denoted as STO-An in Supplementary Materials, Figure S1) were carried out. The almost perfect overlap of the statistical distribution of the pop-in data for STO-Ref and STO-An (Figure S1) verifies that a thermal treatment at 700°C in air is not changing the dislocation nucleation in the near-surface region.

Further, the cumulative probability f for the maximum shear stress τ corresponding to the pop-in (Figure 3) can be correlated by[23]:

$$\ln[-\ln(1-f)] = \frac{V}{kT}\tau + \beta \tag{1}$$

where β is a weak function of the shear stress, k is Boltzmann constant, T is the absolute temperature, and V is the activation volume for dislocation nucleation at the onset of pop-in. According to Schuh's model,[49,50] the activation volume can be calculated based on the distribution of maximum shear stresses for the three different samples. By plotting the pop-in data according to Equation (1), the activation volume can be obtained by multiplying the slope (Figure 4) with kT. Take $T = 293$ K, $k = 1.38 \times 10^{-23}$ J/K, and the fitted slope values, the activation volume for dislocation nucleation is calculated to be 4.12 ± 0.16 Å^3 (STO-Ref),

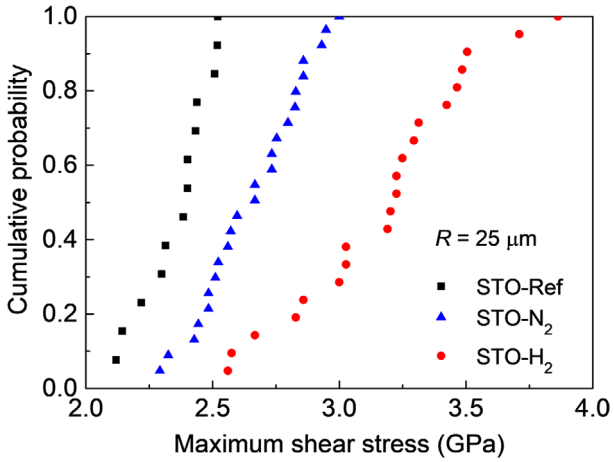

FIGURE 5 Maximum shear stress calculated for the first pop-in event for samples treated under different conditions (i.e., STO-Ref, STO-N_2 and STO-H_2) using an effective indenter tip radius of $R = 25\ \mu$m

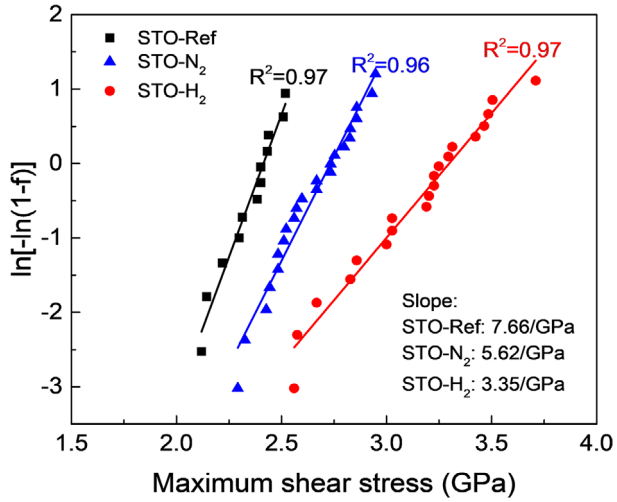

FIGURE 6 Plot of ln[-ln(1-*f*)] as a function of the maximum shear stress τ, for all tested samples. The slope is determined by the linear least-squares fitting procedure

4.00 ± 0.20 Å^3 (STO-N_2), and 3.23 ± 0.16 Å^3 (STO-H_2), respectively. The activation volumes in all three cases are consistently smaller than one atomic volume, indicating a single-atom migration for dislocation nucleation.[23] The slightly smaller activation volume in reduced samples suggests the participation of oxygen vacancies (with a smaller volume) in the course of dislocation nucleation. We also note that the value of STO-N_2 lies between that of STO-Ref and STO-H_2, which is expected.

In addition, indentation pop-in tests with a large tip radius ($R = 25\ \mu$m) were performed for comparison with the smaller tip radius, and the distribution of the pop-in stresses for all three samples is demonstrated in Figure 5. By comparing Figures 3 and 5, a general trend is observed: The maximum shear stress for a larger tip radius is much smaller than that of the smaller tip radius. In addition, a reversal in the pop-in stress distribution from nanoscale ($R = 80$ nm) to microscale ($R = 25\ \mu$m) was confirmed for the reference and reduced samples. The term *reversal* is used to describe that for small tip radius ($R = 80$ nm), the pop-in stress distribution is higher for the reference sample than the reduced ones, but it is the other way around for the large indenter tip ($R = 25\ \mu$m). This is similar to that recently reported in single-crystal $SrTiO_3$ by tuning the Sr/Ti ratio.[10] The underlying mechanisms will be rationalized in Section 4.1.

Similar to the approach demonstrated in Figure 4 for indenter tip with $R = 80$ nm, the pop-in stress distribution for $R = 25\ \mu$m is re-plotted in Figure 6 according to Equation (1). With the fitted slopes (in Figure 6), the activation volumes for dislocation nucleation are calculated as 30.97 ± 1.74 Å^3, 22.72 ± 0.93 Å^3, and 13.55 ± 0.57Å^3 for STO-Ref, STO-N_2, and STO-H_2, respectively. We also note that the value of STO-N_2 lies in between that of STO-Ref and STO-H_2 as in the case of smaller indenter tip in Figure 4. The much larger activation volumes calculated for the large indenter tip suggest heterogeneous dislocation nucleation involving multiple atoms/vacancies[23] or motion of pre-existing dislocations. Moreover, it is worth noting that for large indenters, the stress required to activate pre-existing dislocations is much smaller and not necessarily required up to the maximum shear stress.[37] Therefore, using the maximum shear stress would lead to an underestimation of the activation volume, according to Equation (1). Thus, the activation volumes calculated above can be viewed as the lower bound.

3.3 | Nanoindentation creep tests: dislocation motion

During the pop-in process for large indenter tip, the activation and glide of the pre-existing dislocations may become relevant. To this end, the mobility of the pre-existing dislocations in the reference and reduced samples were quantified using nanoindentation creep tests. The complication of crack formation in nanoindentation creep tests was excluded by choosing a small peak load (3 mN in this case), according to Javaid et al.[23] They demonstrated crack-free indentations with a Berkovich indenter for load up to 3 mN, and cracks only started to appear at load larger than 5 mN.

The representative curves for nanoindentation creep displacement and nanoindentation creep strain rate as a function of time are plotted in Figure 7 for all three samples. The averaged (over 10 tests for each condition) indentation creep strain rate as a function of time (Figure 7B)

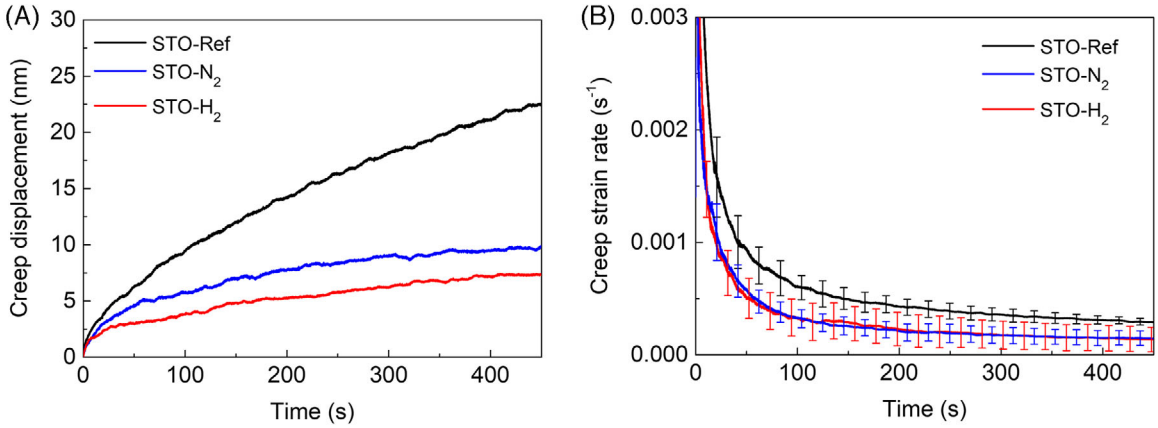

FIGURE 7 (A) Representative nanoindentation creep displacement-time curves. The tests were performed with an indenter radius R = 80 nm for 500 s with a constant load hold of 3 mN. The time $t = 0$ refers to the start of the load holding. (B) Creep strain rate-time curves, the error bars are calculated based on 10 repetitive tests

features a higher creep strain rate of the reference sample than those of the two reduced samples. As the creep time increases, the creep strain rate decreases, approaching an approximately steady-state creep at $t > 400$ s.

The relevant creep mechanisms available at room temperature for single-crystal $SrTiO_3$ are dislocation glide and oxygen vacancy diffusion. The origin of the lower creep strain rate in reduced samples is suggested to lie in the higher oxygen vacancy concentration (Section 3.1). An abundance of oxygen vacancies is suggested to interact with the dislocations and decrease dislocation mobility.

In $SrTiO_3$, cations are immobile at room temperature.[51] Strontium vacancies do not follow the dislocation motion and, hence, cannot result in solute drag. However, with a diffusivity of $D_V = \sim 10^{-13}$ cm^2 s^{-1},[42] oxygen vacancy diffusion is much faster at room temperature. The diffusion length is estimated by $l = \sqrt{D_V t}$. Assuming $t = 10$ s for the time scale for the nanoindentation test, it gives l = 10 nm. Consider the dislocation density under the indenter ($\sim 10^{14}$/m^2),[40] the spacing between the dislocations is about 100 nm. Considering these two length scales, the interaction between the mobile dislocation and the oxygen vacancy is expected during the time and spatial scale in the creep experiment, leading to possible solute strengthening and hence lower mobility of the dislocation in samples with higher oxygen vacancy concentration. Furthermore, the possible charging effect of the mobile dislocations[52] and the oxygen vacancies may lead to a more amplified hardening effect. According to the high-resolution transmission electron microscopy (TEM) characterization of the dislocation cores in $SrTiO_3$ by Gao et al.,[53] the dislocations cores are positively charged, thus a repelling interaction with the positive oxygen vacancies during the dislocation gliding is expected. This argument is further supported by the slight increase in hardness for STO-H_2 (~12.2 GPa) in comparison to STO-Ref (~12.0 GPa) at the same nanoindentation depth of ~400 nm. It is worth mentioning that an analogous mechanism was reported recently for dislocation motion in ZrO_2 where fast oxygen vacancies segregate to dislocations[54] and in hydrogen embrittlement where hydrogen aggregation at dislocations is believed to result in solute drag and hardening.[33,48,55,56]

3.4 | Bulk compression tests

Bei et al.[18] proposed that the mechanical response during indentation with a large spherical indenter could resemble the macroscopic compression behavior. This concept is further validated by the analogous yielding behavior in bulk compression[9] and nanoindentation tests with a large ball indenter ($R = 25\ \mu$m)[10] in single-crystal $SrTiO_3$ with different pre-existing dislocation densities.[37] Here, in order to compare the yielding behavior with the large ball indenter (Figure 5), we further carried out bulk compression for the two extreme cases, that is, reference and forming gas-reduced samples.

The stress-strain curves for bulk compression are presented in Figure 8. The yield strength is determined at the intersection of 0.2% strain due to the lack of a clear yield point in the stress-strain curves. Contrasting the large difference in the yield strength with different pre-existing dislocation densities by Nakamura et al.,[9] the difference in the yield strength between the reference and reduced samples (Figure 8) is marginal. The possible underlying mechanisms for such similar yielding behavior in the bulk deformation for both conditions are discussed later in Section 4. Moreover, the yield strength in the current work is comparable to the previously reported values by various groups. Table 1 summarizes the yield strength

TABLE 1 Summary of yield strength for single-crystal $SrTiO_3$ along [001] direction in bulk compression tests performed at room temperature

	Yield strength (MPa)	Strain rate (s^{-1})	Sample geometry (mm^3)	Pre-existing dislocation density (m^{-2})
Reference (this work)	142–147	10^{-4}	$\sim 2 \times 2 \times 4$	$\sim 10^{10}$
Reduced (this work)	135–142			
Brunner et al.[58]	~ 120	10^{-4}	$2.5 \times 2.5 \times 6$	NA
Brunner[59]	~ 120	2.1×10^{-4}	$2.5 \times 2.5 \times 6$	8×10^{10}
Taeri et al.[60]	~ 140	10^{-4}	$2.5 \times 2.5 \times 6$	8×10^{10}
Yang et al.[57]	45	10^{-4}	$3 \times 3 \times 6$	4.8×10^{13}
Patterson et al.[45]	~ 118	10^{-4}	$4 \times 4 \times 8$	$\sim 10^{12}$
	~ 120	10^{-5}		
Nakamura et al.[9]	119	10^{-5}	$3 \times 3 \times 7.5$	$\sim 10^{10}$
	112	10^{-5}	$3 \times 3 \times 7.5$	$\sim 10^{11}$

Note: The symbol ~ is used for approximation based on the published data unless the values were specified in the references.

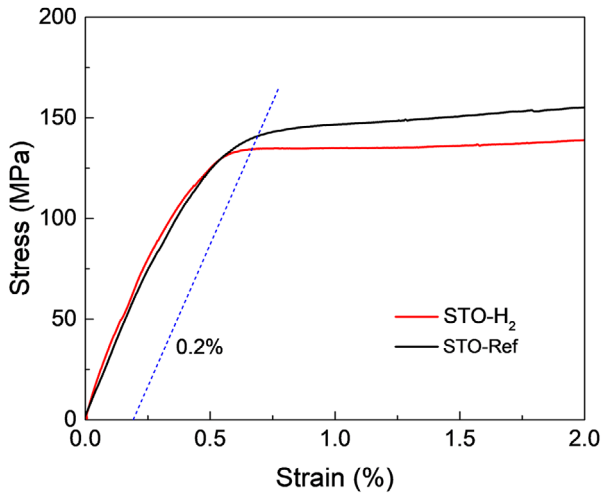

FIGURE 8 Stress-strain curves for bulk compression tests for samples under two different conditions: reference samples (black, STO-Ref) and forming gas-reduced sampled (red, STO-H_2). The strain rate is 10^{-4} s^{-1}

of bulk compression tests on single-crystal $SrTiO_3$ along the [001] orientation (same as in the present work). An anomaly, however, was detected for the yield strength obtained by *Yang* et al.[57] The much smaller yield strength (45 MPa, about a third of the values reported by the others) is most likely due to the exceptionally high pre-existing dislocation density (4.8×10^{13} m^{-2}) in their sample.

4 | DISCUSSION

4.1 | Effect of indenter tip radius on pop-in stress

The effect of tip radius on the pop-in stress exhibits two noticeable features: (i) the pop-in stress for a smaller tip radius (Figure 3 with $R = 80$ nm) is much higher than that with a larger tip radius (Figure 5 with $R = 25\,\mu$m); (ii) a clear reversal of the pop-in stress distribution for the reference and reduced samples is observed for the above two tip radii.

The first feature clearly confirms the indentation pop-in size effect originally identified in single-crystal metals.[27,28] The pop-in size effect is fundamentally different from the traditional indentation size effect in hardness[61] but is related to the stress needed to initiate the incipient plasticity.[27] For a small indenter tip radius ($R = 80$ nm), the stressed volume beneath the indenter tip is correspondingly small and can be dislocation-free[10,37] (see Figure S3 for estimation; practically zero dislocation is found in the stressed volume). This would require normally homogeneous dislocation nucleation[46] to accommodate the incipient plasticity as in the reference sample. With increasing tip radius ($R = 25\ \mu$m), the probability of probing pre-existing dislocations increases[10] (see Figure S3 for estimation; about six pre-existing dislocations in the stressed volume); hence, heterogeneous dislocation nucleation and/or motion of pre-existing dislocations governs the incipient plasticity. In addition, under indentation with the large spherical tip ($R = 25\ \mu$m), the motion of a large number of dislocations might be simultaneously activated, the formation of junctions between which can be largely promoted by the presence of vacancies. The pop-in events may also be caused by the breaking of those junctions and require a higher level of stress than just the lattice friction stress (which is about 90 MPa at room temperature)[62] for dislocation gliding in $SrTiO_3$.

The second feature can be understood by considering the dislocation- point defect interaction within the framework of the indentation pop-in size effect. For a small tip radius, the reduction treatment generates a higher concentration of oxygen vacancies to facilitate dislocation nucleation in a heterogeneous manner, giving lower

pop-in stress when compared to the reference sample (Figure 3). For large tip radius, the abundant oxygen vacancies in reduced samples may accumulate to the space-charged zone of the pre-existing dislocations (as in the case of $SrTiO_3$, it is widely accepted the dislocation cores are oxygen-deficient),[38] suppressing the activation of such dislocations to accommodate the incipient plasticity. Hence, higher pop-in stress is required in the reduced samples.

4.2 | Interaction between dislocations and point defects

First, the nanoscale softening in the oxygen vacancy-rich sample probed by nanoindentation pop-in tests (Figures 2 and 3) agrees well with the previous results by Yavas et al.,[63] who reported a vacancy-induced softening in corroded metallic materials under nanoindentation and analyzed quantitatively by computational simulations at both atomic and continuum level. Unlike in simulation, the fundamental challenge in our current experiment is the accurate quantitative measurement of the vacancy concentration. Instead, a qualitative change of the oxygen vacancy concentration using impedance spectroscopy and nanoindentation pop-in statistics has been analyzed in the current work. In addition, Figure S4 (in Supplementary Materials) does reveal a vacancy gradient effect (higher in the near-surface, lower in the interior in the bulk) on the pop-in statistics, which is very similar to the nanoindentation results by Yavas et al.[63] spacing from the grain boundary to a distance away from it, where higher vacancy concentration is expected near the grain boundary.

Second, during the gliding of dislocations during indentation creep tests (Figure 7), they would interact with point defects (as well as dislocation-dislocation interaction). Such dynamic interaction may lead to dislocation locking and unlocking, leading to fluctuations in the experimental curves (Figure 7) as well as reported in simulation by Xiong et al.[64,65] The possibly charged dislocations may further enhance these fluctuations in ionic crystals during dislocation motion[52] as well as the charged points (e.g., oxygen vacancies). However, the fluctuations observed in the creep displacement-time curves are in the sub-nanometer range and, thus, close to the underlying noise of the displacement signal (< 0.1) of the instrument. Therefore, a more elaborate experimental validation and computational simulation are desirable for investigating the underlying mechanisms.

Moreover, it is noted that the creep strain rate curves for STO-H_2 and STO-N_2 almost overlap with each other (Figure 7B). As discussed above, the mobility of dislocations during the creep tests can be a collective and averaged outcome of the interaction of dislocation-dislocation and dislocation- point defects, which is different from the stage of dislocation nucleation as the incipient or onset of plasticity during indentation pop-in.

4.3 | Yield strength of bulk deformation

At first glance, the negligible difference in the yield strength of bulk deformation for reference and reduced (forming gas) samples seems to contradict the pop-in data from large indenter tip radius.[18] However, a closer examination of the bulk compression samples suggests two possible reasons that might have smeared out the effect of oxygen vacancies on the bulk deformation for the reduced samples.

First of all, the results in Figure S4 (Supplementary Materials) confirm that a gradient of oxygen vacancy concentration in the bulk sample is created by the reduction treatment. The effect of reduction treatment on the pop-in stress decrease is most evident in the near-surface region. While approaching the center of the bulk sample, the effect diminishes and resembles that of the reference sample. Therefore, unlike the large indenter ($R = 25\ \mu$m) that probed the more strongly reduced near-surface region (about several μm beneath the surface, see Section S4 in Supplementary Materials), the reduction effect for the uniaxial bulk compression tests may well have been averaged out.

Second, the bulk samples (about $2 \times 2 \times 4$ mm^3 in dimension) were prepared by cutting an as-received crystal with a dimension of about $4 \times 4 \times 8$ mm^3 using a diamond wire saw. Although the cut surfaces were subsequently polished to reduce the major surface damage from cutting as well as the surface dislocation densities, yet the cutting traces on the sample edges are still visible (Figure S2 in Supplementary Materials). Such cutting traces have been found to be mainly accommodated by dislocations as evidenced by the etch pits after chemically etching the surface perpendicular to the cutting plane (Figure S5 in Supplementary Materials). In addition, fresh dislocations induced by sprinkling the surfaces with fine particles have been found to significantly influence the yield strength in single-crystal MgO (another well-studied ductile oxide).[17] The effect of pre-existing dislocation density on the yield strength of $SrTiO_3$ was also indicated in Table 1 in Section 3, where Yang et al.[57] reported a much lower yield strength due to the much higher pre-existing dislocation density. Considering that both MgO and $SrTiO_3$ have cubic structures and have the same slip systems $\{110\} < 110 >$ at room temperature,[47,66] it is reasonable to assume that the newly induced surface dislocations on the surface of bulk samples from cutting (yet not completely removed during subsequent polishing)

are playing a more dominant role than that of the oxygen vacancies in the bulk deformation. While for the indentation tests, due to the near-surface probed volume and hence limited number of dislocations (see evaluation in Figure S3), the vacancies are playing a more evident role in affecting the dislocation behavior. Such a gap between the nanoindentation and bulk tests has been discussed to be attributed to the different dominating dislocation activities at the nano-/microscale (dislocation nucleation/motion) and the macroscale (dislocation motion/multiplication).[37]

5 | CONCLUSION

The tunable nano-/microscale yielding behavior (i.e., the incipient plasticity) of single-crystal $SrTiO_3$ is demonstrated by *defect chemistry engineering* and nanoindentation tests. The reduction treatment for $SrTiO_3$ increases the oxygen vacancy concentration, which promotes dislocation nucleation at the nanoscale as evidenced by the lower pop-in stress using a sharp indenter (tip radius $R = 80$ nm). On the other hand, the nanoindentation creep tests suggest that the dislocation mobility in the oxygen vacancy-rich samples is decreased, most likely due to a solute drag effect of the oxygen vacancies acting on the dislocations. Contrary to the evident change of the dislocation-based mechanical properties at the nano-/microscale, the yield strength for samples in bulk compression exhibits a negligible difference in the current experiment. Such a gap may be attributed to the different dominating dislocation activities at the nano-/microscale (dislocation nucleation/motion) and the macroscale (dislocation motion/multiplication). Contrasting the noticeable change of the yield strength due to the simultaneous modification of both dislocation density and point defect concentration,[9,10] the effect of point defects in the current reduction treatment is most evident at the nano-/microscale but negligible for macroscale deformation. Our work suggests that the reduction treatment may be a more effective approach for tuning the dislocation plasticity at a small scale for potential nano-/microscale devices.

ACKNOWLEDGMENTS

Xufei Fang acknowledges the helpful discussion with Prof. Atsutomo Nakamura (Osaka University) and the financial support by the Athene Young Investigator Programme at TU Darmstadt. Kuan Ding thanks the DFG for financial support (No. 418649505). Qaisar Khushi Muhammad acknowledges funding from Deutscher Akademischer Austauschdienst (DAAD) for the fellowship with award number 91669061. Karsten Durst acknowledges the funding by DFG (DU 424/11-1). Jürgen Rödel acknowledges the financial support by DFG (No. 414179371). Wolfgang Rheinheimer acknowledges funding by the DFG (RH 146/1). The constructive and insightful comments by the two anonymous reviewers during the review process of this work are also gratefully acknowledged.

Open access funding enabled and organized by Projekt DEAL.

CONFLICT OF INTEREST

The authors declare that they have no conflict of interest.

ORCID

Qaisar Khushi Muhammad https://orcid.org/0000-0002-6976-7651
Lukas Porz https://orcid.org/0000-0003-3163-085X
Till Frömling https://orcid.org/0000-0002-8827-1926
Xufei Fang https://orcid.org/0000-0002-3887-0111

REFERENCES

1. Adepalli KK, Kelsch M, Merkle R, Maier J. Influence of line defects on the electrical properties of single crystal TiO_2. Adv Funct Mater. 2013;23(14):1798–806.
2. Muhammad QK, Porz L, Nakamura A, Matsunaga K, Rohnke M, Janek J, Rödel J, Frömling T. Donor and acceptor-like self-doping by mechanically induced dislocations in bulk TiO_2. Nano Energy. 2021;85:105944.
3. Khafizov M, Pakarinen J, He L, Hurley DH. Impact of irradiation induced dislocation loops on thermal conductivity in ceramics. J Am Ceram Soc. 2019;102(12):7533–42.
4. Abdellaoui L, Chen Z, Yu Y, Luo T, Hanus R, Schwarz T, et al. Parallel dislocation networks and cottrell atmospheres reduce thermal conductivity of PbTe Thermoelectrics. Adv Funct Mater. 2021;31(20):2101214.
5. Johanning M, Porz L, Dong J, Nakamura A, Li J-F, Rödel J. Influence of dislocations on thermal conductivity of strontium titanate. Appl Phys Lett. 2020;117(2):021902.
6. Höfling M, Zhou X, Riemer LM, Bruder E, Liu B, Zhou L, et al. Control of polarization in bulk ferroelectrics by mechanical dislocation imprint. Science. 2021;372:961–4.
7. Li J, Wang H, Zhang X. Nanoscale stacking fault–assisted room temperature plasticity in flash-sintered TiO_2. Sci Adv. 2019;5:eaaw5519.
8. Phuah XL, Cho J, Tsakalakos T, Mukherjee AK, Wang H, Zhang X. Defects in flash-sintered ceramics and their effects on mechanical properties. MRS Bull. 2021;46:44–51.
9. Nakamura A, Yasufuku K, Furushima Y, Toyoura K, Lagerlöf K, Matsunaga K. Room-temperature plastic deformation of strontium titanate crystals grown from different chemical compositions. Crystals. 2017;7(11):351.
10. Fang X, Ding K, Janocha S, Minnert C, Rheinheimer W, Frömling T, et al. Nanoscale to microscale reversal in room-temperature plasticity in $SrTiO_3$ by tuning defect concentration. Scr Mater. 2020;188:228–32.
11. Moon W-J, Saka H. Toughening of a brittle material by means of dislocation subboundaries. Philos Mag Lett. 2000;80(7):461–6.
12. Porz L, Klomp AJ, Fang X, Li N, Yildirim C, Detlefs C, et al. Dislocation-toughened ceramics. Mater Horiz. 2021;8:1528.

13. Zhu T, Ding K, Oshima Y, Amiri A, Bruder E, Stark RW, et al. Switching the fracture toughness of single-crystal ZnS using light irradiation. Appl Phys Lett. 2021;118:154103
14. Gilman JJ. Dislocation sources in crystals. J Appl Phys. 1959;30:1584.
15. Johnston WG, Gilman JJ. Dislocation multiplication in lithium fluoride crystals. J Appl Phys. 1960;31(4):632–43.
16. Michot G, Loyola de Oliveira MA, Koizumi H. Size scale effects on brittle to ductile transition. Le Journal de Physique IV. 1998;08:145–54.
17. Stokes RJ, Li CH. Dislocations and the tensile strength of magnesium oxide. J Am Ceram Soc. 1963;46(9):423–34.
18. Bei H, Xia YZ, Barabash RI, Gao YF. A tale of two mechanisms: Strain-softening versus strain-hardening in single crystals under small stressed volumes. Scr Mater. 2016;110:48–52.
19. Maier J. Defect chemistry: Composition, transport, and reactions in the solid state; part I: Thermodynamic. Angew Chem. 1993;32:313–35.
20. Gunkel F, Christensen DV, Chen YZ, Pryds N. Oxygen vacancies: The (in)visible friend of oxide electronics. Appl Phys Lett. 2020;116:120505.
21. Hirth JP, Lothe J. *Theory of dislocations*. 2nd ed. Malabar, Florida: John Wiley & Sons, Inc.; 1982.
22. Dai FZ, Zhou Y. Reducing the ideal shear strengths of ZrB_2 by high efficient alloying elements (Ag, Au, Pd and Pt). Sci Rep. 2017;7:43416.
23. Gan K, Yan D, Zhu S, Li Z. Interstitial effects on the incipient plasticity and dislocation behavior of a metastable high-entropy alloy: nanoindentation experiments and statistical modeling. Acta Mater. (2021) 116633.
24. Ye YX, Ouyang B, Liu CZ, Duscher GJ, Nieh TG. Effect of interstitial oxygen and nitrogen on incipient plasticity of NbTiZrHf high-entropy alloys. Acta Mater. 2020;199:413–24.
25. Salehinia I, Bahr DF. The impact of a variety of point defects on the inception of plastic deformation in dislocation-free metals. Scr Mater. 2012;66(6):339–42.
26. Jin K, Xia Y, Crespillo M, Xue H, Zhang Y, Gao YF, Bei H. Quantifying early stage irradiation damage from nanoindentation pop-in tests. Scr Mater. 2018;157:49–53.
27. Shim S, Bei H, George EP, Pharr GM. A different type of indentation size effect. Scr Mater. 2008;59(10):1095–8.
28. Morris JR, Bei H, Pharr GM, George EP. Size effects and stochastic behavior of nanoindentation pop in. Phys Rev Lett. 2011;106(16):165502.
29. Li J, Vliet KJV, Zhu T, Yip S, Suresh S. Atomistic mechanisms governing elastic limit and incipient plasticity in crystals. Nature. 2002;418:307–10.
30. Li J, Dehm G, Kirchlechner C. How close can indents be placed without risking an erroneous pop-in statistics? Materialia. 2019;7:100378.
31. Fang X, Bishara H, Ding K, Tsybenko H, Porz L, Höfling M, et al. Nanoindentation pop-in in oxides at room temperature: dislocation activation or crack formation? J Am Ceram Soc. 2021;104:4728–41.
32. Kirchheim R. Solid solution softening and hardening by mobile solute atoms with special focus on hydrogen. Scr Mater. 2012;67(9):767–70.
33. Fang X, Kreter A, Rasinski M, Kirchlechner C, Brinckmann S, Linsmeier C, et al. Hydrogen embrittlement of tungsten induced by deuterium plasma: Insights from nanoindentation tests. J Mater Res. 2018;33(20):3530–6.
34. Li H, Ngan AHW. Size effects of nanoindentation creep. J Mater Res. 2003;19(2):513–22.
35. Prach O, Minnert C, Johanns KE, Durst K. A new nanoindentation creep technique using constant contact pressure. J Mater Res. 2019;34(14):2492–500.
36. Nakamura A, Fang X, Matsubara A, Tochigi E, Oshima Y, Saito T, et al. Photoindentation: A new route to understanding dislocation behavior in light. Nano Lett. 2021;21:1962–7.
37. Fang X, Porz L, Ding K, Nakamura A. Bridging the gap between bulk compression and indentation test on room-temperature plasticity in oxides: Case study on $SrTiO_3$. Crystals. 2020;10(10):933–47.
38. Souza RAD. Transport properties of dislocations in $SrTiO_3$ and other perovskites. Curr Opin Solid State Mater Sci. 2021;25:100923.
39. Maier V, Merle B, Göken M, Durst K. An improved long-term nanoindentation creep testing approach for studying the local deformation processes in nanocrystalline metals at room and elevated temperatures. J Mater Res. 2013;28(09):1177–88.
40. Javaid F, Bruder E, Durst K. Indentation size effect and dislocation structure evolution in (001) oriented $SrTiO_3$ Berkovich indentations: HR-EBSD and etch-pit analysis. Acta Mater. 2017;139:1–10.
41. Oliver WC, Pharr GM. An improved technique for determining hardness and elastic modulus using load and displacement sensing indentation experiments. J Mater Res. 1992;7(6):1564–83.
42. De Souza RA. Oxygen diffusion in $SrTiO_3$ and related perovskite oxides. Adv Funct Mater. 2015;25(40):6326–42.
43. Ye K, Li K, Lu Y, Guo Z, Ni N, Liu H, et al. An overview of advanced methods for the characterization of oxygen vacancies in materials. Trends Anal Chem. 2019;116:102–8.
44. Johnson KL. *Contact Mechanics*. Cambridge, London: Cambridge University Press; 1985.
45. Patterson EA, Major M, Donner W, Durst K, Webber KG, Rödel J. Temperature-dependent deformation and dislocation density in $SrTiO_3$ (001) single crystals. J Am Ceram Soc. 2016;99(10):3411–20.
46. Lorenz D, Zeckzer A, Hilpert U, Grau P, Johansen H, Leipner HS. Pop-in effect as homogeneous nucleation of dislocations during nanoindentation. Phys Rev B. 2003;67(17):172101.
47. Javaid F, Stukowski A, Durst K. 3D Dislocation structure evolution in strontium titanate: Spherical indentation experiments and MD simulations. J Am Ceram Soc. 2017;100(3):1134–45.
48. Barnoush A, Asgari M, Johnsen R. Resolving the hydrogen effect on dislocation nucleation and mobility by electrochemical nanoindentation. Scr Mater. 2012;66(6):414–7.
49. Mason JK, Lund AC, Schuh CA. Determining the activation energy and volume for the onset of plasticity during nanoindentation. Phys Rev B. 2006;73(5):054102.
50. Schuh CA, Mason JK, Lund AC. Quantitative insight into dislocation nucleation from high-temperature nanoindentation experiments. Nat Mater. 2005;4(8):617–21.
51. Gömann K, Borchardt G, Schulz M, Gömann A, Maus-Friedrichs W, Lesage B, et al. Sr diffusion in undoped and

La-doped $SrTiO_3$ single crystals under oxidizing conditions. Phys Chem Chem Phys. 2005;7(9):2053–60.
52. Whitworth RW. Charged dislocations in ionic crystals. Adv Phys. 1975;24(2):203–304.
53. Gao P, Ishikawa R, Feng B, Kumamoto A, Shibata N, Ikuhara Y. Atomic-scale structure relaxation, chemistry and charge distribution of dislocation cores in $SrTiO_3$. Ultramicroscopy. 2018;184(Pt A):217–24.
54. Cho J, Li J, Wang H, Li Q, Fan Z, Mukherjee AK, et al. Study of deformation mechanisms in flash-sintered yttria-stabilized zirconia by in-situ micromechanical testing at elevated temperatures. Mater Res Lett. 2019;7(5):194–202.
55. Duarte MJ, Fang X, Rao J, Krieger W, Brinckmann S, Dehm G. In situ nanoindentation during electrochemical hydrogen charging: a comparison between front-side and a novel back-side charging approach. J Mater Sci. 2021;56:8732–44.
56. Fang X, Rasinski M, Kreter A, Kirchlechner C, Linsmeier C, Dehm G, et al. Plastic deformation of tungsten due to deuterium plasma exposure: Insights from micro-compression tests. Scr Mater. 2019;162:132–5.
57. Yang K-H, Ho N-J, Lu H-Y. Plastic deformation of <001>single-crystal $SrTiO_3$ by compression at room temperature. J Am Ceram Soc. 2011;94(9):3104–11.
58. Brunner D, Taeri-Baghbadrani S, Sigle W, Rühle M. Surprising results of a study on the plasticity in strontium titanate. J Am Ceram Soc. 2001;84(5):1161–3.
59. Brunner D. Low-temperature plasticity and flow-stress behaviour of strontium titanate single crystals. Acta Mater. 2006;54(19):4999–5011.
60. Taeri S, Brunner D, Sigle W, Rühle M. Deformation behaviour of strontium titanate between room temperature and 1800 K under ambient pressure. Z Mettllkd. 2004;95(6):433–46.
61. Gao H, Nix WD. Indentation size effects in crystalline materials: a law for strain gradient plasticity. J Mech Phys Solids. 1998;46(3):411–25.
62. Javaid F, Johanns KE, Patterson EA, Durst K. Temperature dependence of indentation size effect, dislocation pile-ups, and lattice friction in (001) strontium titanate. J Am Ceram Soc. 2018;101(1):356–64.
63. Yavas D, Phan T, Xiong L, Hebert KR, Bastawros AF. Mechanical degradation due to vacancies produced by grain boundary corrosion of steel. Acta Mater. 2020;200:471–80.
64. Xiong LM, Chen YP, Lee JD. Atomistic measure of the strength of MgO nanorods. Theor Appl Fract Mech. 2006;46(3):202–8.
65. Xiong L, Chen Y. Multiscale modeling and simulation of single-crystal MgO through an atomistic field theory. Int J Solids Struct. 2009;46(6):1448–55.
66. Amodeo J, Merkel S, Tromas C, Carrez P, Korte-Kerzel S, Cordier P, et al. Dislocations and plastic deformation in MgO crystals: A review. Crystals. 2018;8(6):240–92.

SUPPORTING INFORMATION

Additional supporting information may be found in the online version of the article at the publisher's website.

How to cite this article: Stich S, Ding K, Muhammad QK, Porz L, Minnert C, Rheinheimer W, et al. Room-temperature dislocation plasticity in $SrTiO_3$ tuned by defect chemistry. J Am Ceram Soc. 2022;105:1318–1329. https://doi.org/10.1111/jace.18118